Journal of the Mechanics and Physics of Solids 125 (2019) 749–761

Contents lists available at ScienceDirect

Journal of the Mechanics and Physics of Solids

journal homepage: www.elsevier.com/locate/jmps

Tearing a hydrogel of complex rheology

Ruobing Bai[1], Baohong Chen[1], Jiawei Yang, Zhigang Suo*

John A. Paulson School of Engineering and Applied Sciences, Kavli Institute for Bionano Science and Technology, Harvard University, Cambridge, MA 02138, USA

ARTICLE INFO

Article history:
Received 5 November 2018
Revised 31 December 2018
Accepted 26 January 2019
Available online 1 February 2019

Keywords:
Hydrogel
Slow crack
Rheology
Tear
Fatigue

ABSTRACT

Tough hydrogels of many chemical compositions are being discovered, and are opening new applications in medicine and engineering. To aid this rapid and worldwide development, it is urgent to study these hydrogels at the interface between mechanics and chemistry. A tough hydrogel often deforms inelastically over a large volume of the sample used in a fracture experiment. The rheology of the hydrogel depends on chemistry, and is usually complex, which complicates the crack behavior. This paper studies a hydrogel that has two interpenetrating networks: a polyacrylamide network of covalent crosslinks, and an alginate network of ionic (calcium) crosslinks. When the hydrogel is stretched, the polyacrylamide network remains intact, but the alginate network partially unzips. We tear a thin layer of the hydrogel at speed v and measure the energy release rate G. The v–G curve depends on the thickness of the hydrogel for thin hydrogels, and is independent of the thickness of the hydrogel for thick hydrogels. The energy release rate approaches a threshold, below which the tear speed vanishes. The threshold depends on the concentration of calcium. The threshold may also depend on the thickness when the thickness is comparable to the size of inelastic zone. The threshold determined by slow tear differs from the threshold determined by cyclic fatigue. We discuss these experimental findings in terms of the mechanics of tear and the chemistry of the hydrogel.

1. Introduction

Hydrogels are molecular aggregates of polymers and water. Most tissues of animals and plants are hydrogels. Whereas the biological hydrogels date back to the beginning of life on Earth, synthetic hydrogels are relatively new materials. The first family of synthetic hydrogels was described in a patent granted in 1961 (Wichterle and Lim, 1961). In principle, synthetic hydrogels can mimic biological tissues—chemically, mechanically, and electrically—to arbitrary degree of fidelity. From the very beginning the inventors recognized the potential of synthetic hydrogels for biological use (Wichterle and Lim, 1960). Worldwide development of hydrogels followed immediately and has been vibrant since. Familiar consumer products of hydrogels include contact lenses (Caló and Khutoryanskiy, 2015) and superabsorbent diapers (Masuda, 1994). Medical applications include drug delivery (Li and Mooney, 2016), wound dressing (Li et al., 2017a), and tissue repair (Zhang and Khademhosseini, 2017). Potential non-medical applications of hydrogels have also emerged recently. Many hydrogels are

* Corresponding author.
E-mail address: suo@seas.harvard.edu (Z. Suo).
[1] These authors contributed equally to this work.

https://doi.org/10.1016/j.jmps.2019.01.017
0022-5096/

stretchable, transparent, ionic conductors (Keplinger et al., 2013). A large number of potential non-medical applications belong to ionotronics, devices that function on the basis of both mobile ions and mobile electrons (Yang and Suo, 2018). Examples include artificial muscles (Acome et al., 2018; Kellaris et al., 2018; Keplinger et al., 2013; Li et al., 2017b), artificial skins (Lei et al., 2017; Sarwar et al., 2017; Sun et al., 2014), artificial axons (Le Floch et al., 2017; Yang et al., 2015), artificial eels (Schroeder et al., 2017), touchpads (Kim et al., 2016), triboelectric generators (Parida et al., 2017; Pu et al., 2017; Xu et al., 2017), liquid crystal devices (Yang et al., 2017), and ionotronic luminescent devices (Larson et al., 2016; Yang et al., 2016a). Other applications include soft robots (Yuk et al., 2017), water matrix composites (Huang et al., 2017; Illeperuma et al., 2014; Lin et al., 2014), optical fibers (Choi et al., 2015; Guo et al., 2016), chemical sensors (Qin et al., 2018; Sun et al., 2018), and fire-retarding blankets (Illeperuma et al., 2016).

In the invention of Wichterle and Lim (1961), each hydrogel aggregates a large amount of water and a sparse polymer network. Within the hydrogel, water molecules act as a liquid of low viscosity, changing neighbors constantly, and transmitting force negligibly. The sparse polymer network acts as an entropic spring, having covalent crosslinks, and transmitting force over long distances. Such a single-network hydrogel has a simple rheology: near-perfect elasticity of a large limiting stretch. (In this paper we neglect the migration of water in the hydrogel.) The near-perfect elasticity makes the hydrogel brittle; for example, the fracture energy of a polyacrylamide hydrogel is $\sim 100\,\mathrm{J/m^2}$ (Sun et al., 2012), much lower than the fracture energies of biological tissues such as cartilage and ligament ($\sim 1000\,\mathrm{J/m^2}$), or the fracture energies of engineering materials such as natural rubber ($\sim 10{,}000\,\mathrm{J/m^2}$). A brittle hydrogel is flaw-sensitive—that is, the hydrogel has a large limiting stretch when containing small flaws, but ruptures at a small stretch when containing a large flaw (Chen et al., 2017).

Gong et al. (2003) discovered a synthetic hydrogel as tough as cartilage. This discovery has launched the worldwide development of tough hydrogels of many chemical compositions (Creton, 2017; Du et al., 2014; Gong, 2010; Haque et al., 2012a,b; Hu et al., 2015; Jeon et al., 2016; Sun et al., 2012; Sun et al., 2013; Yang et al., 2013, 2016b; Zhang et al., 2015; Zhang and Khademhosseini, 2017; Zhao, 2014). In the discovery of Gong et al. (2003), the tough hydrogel has two polymer networks, one being more stretchable than the other. The two polymer networks interpenetrate, in topological entanglement. Both networks must break when a crack extends in the hydrogel. More significantly, the more stretchable network transmits the intense stress from the front of the crack into the bulk of the hydrogel. Away from the crack front, the more stretchable network remains intact, but the less stretchable network ruptures in many places. The damage is distributed over a large volume of the hydrogel, and dissipates a great amount of energy.

As tough hydrogels and their applications are being developed rapidly worldwide, it is urgent to study these hydrogels at the interface between mechanics and chemistry. A double-network hydrogel achieves high toughness through the synergy of two processes: the decohesion of the more stretchable network at the front of the crack, and the dissipation of the less stretchable network in the bulk of the hydrogel. The mechanics of this decohesion-dissipation synergy is reminiscent of toughening mechanisms in other materials, including metals, plastics, ceramics, and composites (e.g., Evans, 1990). The chemistry of the synergy, however, is distinct in each class of materials. In the double-network hydrogel, we call the more stretchable network the *primary network*, and the less stretchable network a *toughener*. By a toughener we mean a constituent of a hydrogel that can cause pronounced inelasticity (e.g., viscosity, plasticity, and distributed damage). A large variety of tougheners have led to hydrogels of complex rheology, which in turn have led to observable effects in fracture. Examples include rate-dependent fracture (Baumberger et al., 2006a,b; Baumberger and Ronsin, 2009, 2010; Lefranc and Bouchaud, 2014; Seitz et al., 2009; Sun et al., 2017; Tanaka et al., 2000, 2005), creep fracture (Karobi et al., 2016), delayed fracture (Bonn et al., 1998; Tang et al., 2017; Wang and Hong, 2012), and fatigue fracture (Bai et al., 2018, 2017; Tang et al., 2017; Zhang et al., 2018a; Zhang et al., 2018b,c). Despite recent attempts (Long and Hui, 2015, 2016; Mao and Anand, 2018; Noselli et al., 2016; Qi et al., 2018; Yu et al., 2018; Zhang et al., 2015), hydrogels of complex rheology are inadequately studied to link the mechanics of fracture to the chemistry of hydrogels. In particular, in a fracture experiment, when a large volume in the sample deforms inelastically, the measured fracture energy is no longer a material constant, but depends on the type of specimen and the speed of crack. For further background, see our recent review on fatigue of hydrogels (Bai et al., 2019).

This paper uses a polyacrylamide-calcium-alginate (PAAm-Ca-alginate) hydrogel as a model material to study the effect of rheology on fracture under the conditions of both small-scale and large-scale inelasticity. The hydrogel has two interpenetrating networks: a polyacrylamide network of covalent crosslinks, and an alginate network of ionic (calcium) crosslinks. When the hydrogel is stretched, the polyacrylamide network remains intact, but the alginate network partially unzips. A stress relaxation test shows that the calcium-crosslinked alginate hydrogel exhibits solid-like rheology. We tear a thin layer of the PAAm-Ca-alginate hydrogel at speed v and measure the tear force. Tear is a convenient experimental setup to study time-dependent rupture of a hydrogel of complex rheology. The hydrogel is attached with two inextensible backing layers, which guide the crack to extend along the midline of the hydrogel, and localize the active deformation in a region scaled by the thickness of the hydrogel. The active region of deformation travels at the tear speed. Furthermore, the measured tear force gives the energy release rate G, independent of the rheology of the hydrogel. The v–G curve depends on both the thickness of the hydrogel and the concentration of calcium. The energy release rate approaches a threshold, below which the tear speed vanishes. The threshold depends on the concentration of calcium. The threshold may also depend on the thickness when the thickness is comparable to the size of inelastic zone. The threshold determined by slow tear differs from the threshold determined by cyclic fatigue. We interpret these experimental findings in terms of the mechanics of tear and the chemistry of the hydrogel.

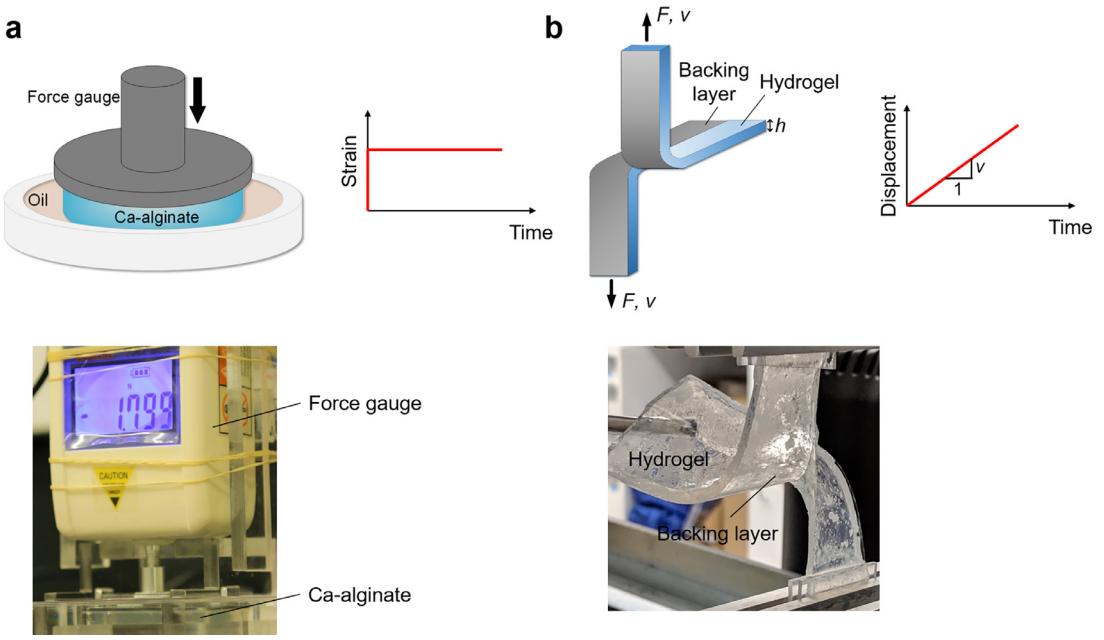

Fig. 1. Experimental setups. (a) The stress relaxation test. (b) The tear test.

2. Experimental section

2.1. Preparation of hydrogels

We purchased from Sigma Aldrich the following chemicals: acrylamide (AAm, A8887), *N*,*N*′-methylenebis(acrylamide) (MBAA, M7279), *N*,*N*,*N*′,*N*′-tetramethylethylenediamine (TEMED, T7024), ammonium persulfate (APS, A9164), and calcium sulfate dihydrate ($CaSO_4 \cdot 2H_2O$, C3771). We purchased sodium alginate (Manugel GMB) from FMC Biopolymer. All chemicals were received and used without further purification.

To prepare the PAAm-Ca-alginate hydrogel, we dissolved AAm powders of 40.54 g and sodium alginate powders of 6.76 g in 300 mL deionized water to form an aqueous solution. We then added MBAA, TEMED, APS and $CaSO_4 \cdot 2H_2O$ in quantities of 0.0012, 0.0025, 0.0042 and 0.022 times the weight of AAm in sequence. The solution was completely mixed, degassed and injected into acrylic molds of 40 mm width, 90 mm length and variable thickness, and covered with an acrylic plate. The samples were then stored at room temperature for more than 18 h for complete polymerization. To study the effect of sample thickness, we prepared samples with thickness of 0.4 mm, 0.7 mm, 1.0 mm, 1.5 mm and 3.0 mm, measured after the polymerization.

To prepare the ionically crosslinked Ca-alginate hydrogel, we dissolved sodium alginate powders of 6.76 g in 300 mL deionized water to form an aqueous solution. We then added $CaSO_4 \cdot 2H_2O$ of 0.9 g, the same amount as used in preparing the PAAm-Ca-alginate hydrogel above (0.022 times the weight of AAm). The solution was completely mixed, degassed and injected into cylindrical acrylic molds of 6 mm height and 3 cm diameter, covered with an acrylic plate. The samples were stored at room temperature for more than 18 h for complete polymerization.

To study the effect of calcium in the PAAm-Ca-alginate hydrogel, we modified the amount of $CaSO_4 \cdot 2H_2O$ in the solution. We synthesized three types of PAAm-alginate hydrogels, and named them *0-Ca, 1-Ca* and *2-Ca*. The 0-Ca hydrogel corresponds to no $CaSO_4 \cdot 2H_2O$ added to the solution, the 1-Ca hydrogel corresponds to 0.9 g $CaSO_4 \cdot 2H_2O$ (0.022 times the weight of AAm), and the 2-Ca hydrogel corresponds to 1.8 g $CaSO_4 \cdot 2H_2O$ (0.044 times the weight of AAm).

2.2. Stress relaxation test

The prepared Ca-alginate hydrogel cylinder was compressed with a force gauge (HF-50N, M&A Instrument, Inc.) at a fixed compressive strain of 20% (Fig. 1a). The hydrogel and the force gauge were firmly mounted on a homemade acrylic mold. The hydrogel and the attaching end of the force gauge were completely immersed in silicone oil to avoid dehydration. Negligible buoyance force was observed by the force gauge. The whole setup was kept undisturbed for 12 days, with the compressive force measured every day. The nominal stress is defined by the compressive force divided by the area of the Ca-alginate hydrogel in the undeformed state.

2.3. Tear test

Each sample of the PAAm-Ca-alginate hydrogel was 40 mm in width and 90 mm in length. We glued inextensible backing layers (clear polyester film, McMaster-Carr), of thickness 100 μm, width 20 mm and length 90 mm, on the top and bottom surfaces of the hydrogel (grey area in Fig. 1b) using the Krazy glue. We cut each backing layer to form a long rectangular shape, and covered half of each surface of the sample, with no observable gap between the long edges of the backing layers. Afterwards, we used razor blades to cut an initial crack of 20 mm along the midline of the hydrogel, forming two arms of 20 mm width and 20 mm length. The two arms were then fixed by the grips of a tensile testing machine (Instron 5966) with a 10 N load cell. During tear, the machine maintained a constant loading speed and recorded the force (Fig. 1b). In experiments, we did not observe any significant difference in the force-displacement curve when attaching stiff backing layers on both sides of the sample, although we did not systematically study the effect of different ways of applying the backing layers.

To prevent dehydration of the hydrogel during a test with low loading speed (<0.1 mm/s), a humidity chamber was made to cover the entire sample and the grips. The humidity chamber was home-made with acrylic sheets, equipped with a commercial humidifier and a humidity control system (Zoo med, HygroTherm Humidity and Temperature Controller). The relative humidity in the chamber was maintained at above 95%. All the samples were weighed before and after the test, and no more than 5% weight was lost.

3. Toughers of solid-like or liquid-like rheology

Emphasis of this work will be placed on the near-threshold behavior, as the tear speed approaches zero. To this end, we need to know the long-time stress-relaxation behavior of the hydrogel. The hydrogel has two interpenetrating polymer networks, one being more stretchable than the other. As noted before, we call the more stretchable network the *primary network*, and call the less stretchable network the *toughener*. In a rheological model, the primary network and the toughener are in parallel, representing the interpenetrating topology of the two networks (Fig. 2a).

We represent the primary network by a spring. Because the primary network has covalent crosslinks, the hydrogel behaves like an elastomer, and has a limiting stretch. The limiting stretch also prevails at the crack front in the hydrogel. By contrast, a metal or an uncrosslinked plastic can flow by arbitrarily large strain, so long as the deformation does not cause instability, such as necking or voiding.

We classify the toughener into two types (Fig. 2b). The toughener is a polymer network crosslinked by sacrificial bonds. Under a constant strain, a liquid-like toughener, represented by a spring in series with a dashpot, cannot sustain any force as time approaches infinity, corresponding to complete dissociation of the sacrificial bonds. A solid-like toughener, represented by a spring in parallel with a dashpot, sustains a finite force as time approaches infinity, corresponding to incomplete dissociation of the sacrificial bonds.

The model material chosen for this study is the polyacrylamide-calcium-alginate (PAAm-Ca-alginate) hydrogel discovered by Sun et al. (2012). In this hydrogel, the primary network is the covalently crosslinked PAAm, and the toughener is the ionically crosslinked Ca-alginate (Fig. 3). A PAAm hydrogel has a fracture toughness of about 100 J/m^2. A Ca-alginate hydrogel has a fracture toughness of about 10 J/m^2. Both hydrogels are brittle compared to natural rubber, but combining them together creates the tough hydrogel with fracture toughness over 10,000 J/m^2 (Li et al., 2014; Sun et al., 2012). The PAAm-Ca-alginate hydrogel is as stretchable as the PAAm hydrogel and as stiff as the Ca-alginate hydrogel. Since its creation, the hydrogel has been actively studied and developed for applications including soft robots (Yuk et al., 2017), tough adhesives

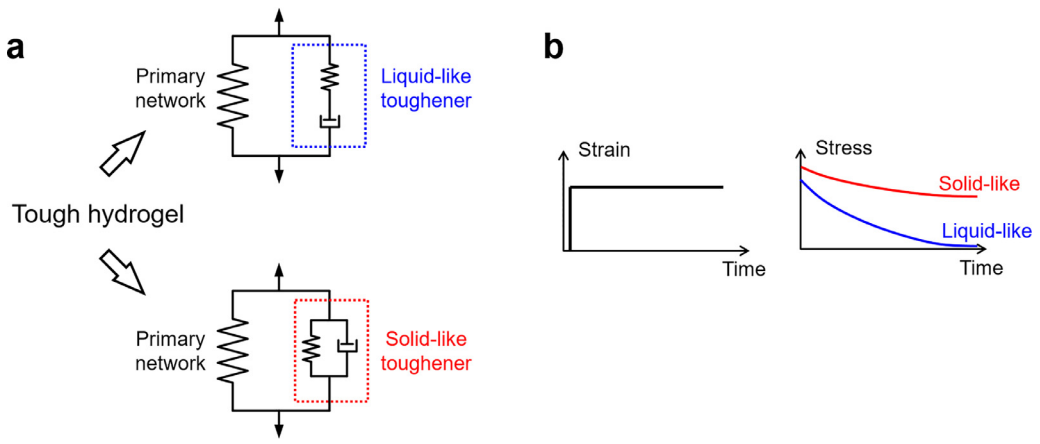

Fig. 2. Rheological models of a tough hydrogel. (a) The primary network is represented by an elastic spring. The toughener is represented by an elastic spring with a dashpot. (b) Stress relaxation of solid-like and liquid-like toughers.

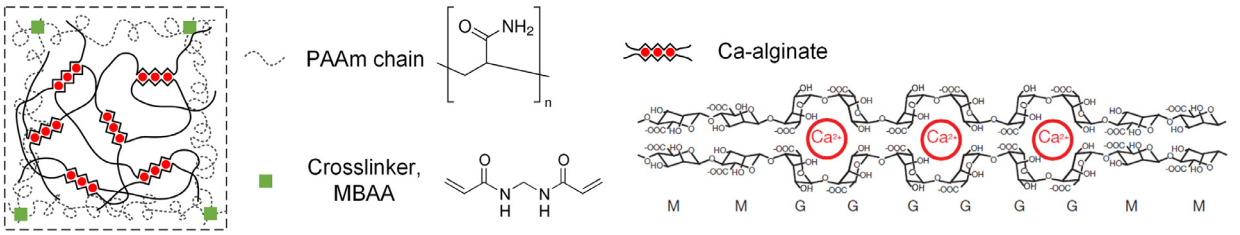

Fig. 3. Molecular picture of a PAAm-Ca-alginate hydrogel.

(Li et al., 2017a), and drug delivery systems (Liu et al., 2017). The PAAm-Ca-alginate hydrogels suffer fatigue damage and fatigue fracture under cyclic loads (Bai et al., 2017). The cyclic loads cause the progressive unzipping of the Ca-alginate ionic bonds, and the corresponding reduction of the elastic modulus and toughness over thousands of cycles. Such process is irreversible at room temperature (Sun et al., 2012). Slow crack growth of the PAAm-Ca-alginate hydrogel, however, is studied in the present paper for the first time.

We now focus on the rheology of the toughener, the Ca-alginate. The calcium ions and the alginate chains form ionic bonds in the form of the "egg-box" structure, with the bond energy on the order of kT (Braccini and Pérez, 2001; Sikorski et al., 2007), where kT is the temperature in the unit of energy. This ionic bond is weaker than the covalent bond forming the PAAm network or the alginate chains by two orders of magnitude. Such a weak bond makes the Ca-alginate network unzip under a relatively small force over a long enough time, leading to pronounced inelasticity (Mao et al., 2017; Zhao et al., 2010). Stress relaxation of the pure Ca-alginate hydrogel has been conducted (Mitchell and Blanshard, 1976; Zhao et al., 2010). However, it is yet unclear whether the Ca-alginate network is liquid-like or solid-like, due to the known degradation of Ca-alginate induced by ion exchange or bacteria (Bajpai and Sharma, 2004; Hashimoto et al., 2005) in the aqueous testing environment such as phosphate-buffered saline (PBS). The degradation may have damaged the network over the relaxation test before the mechanically induced unzipping takes place.

To examine the rheology of the Ca-alginate network of the current composition, we conducted our own stress relaxation test by applying a compressive strain of 20% to a Ca-alginate hydrogel immersed in silicone oil, in order to prevent any solvent or ion exchange. The stress level was about 6.5 kPa at the beginning, gradually decreased to about 2 kPa, and almost reached a plateau after about 12 days (Fig. 4). The significant reduction of stress level indicates the slow unzipping of Ca-alginate ionic bonds. The finite plateau over a long time indicates the solid-like behavior of the Ca-alginate toughener. This result indicates that, although each ionic bond is weak, the large number of ionic bonds can still lead to a solid-like network.

In a double-network hydrogel, the primary network and the toughener interact. Examples of interactions include bonds between matching functional groups and entanglements between polymer chains of the two networks. In the PAAm-Ca-alginate hydrogel, the PAAm network and Ca-alginate network interpenetrate in topological entanglement, but no appreciable bonds form between the two networks. When the hydrogel is stretched, the PAAm remains intact, and the alginate network partially break by unzipping the ionic crosslinks.

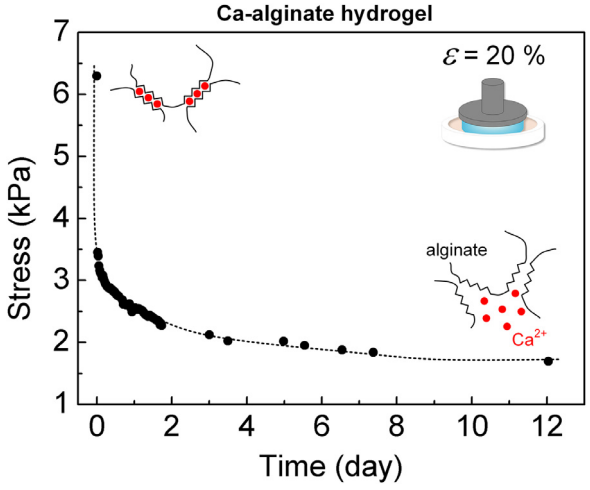

Fig. 4. Stress relaxation of the Ca-alginate hydrogel.

4. Mechanics of tear

Fracture of a material of complex rheology is commonly studied using experiments of slow crack growth. Experimental setups include tear (Gent and Lai, 1994; Greensmith and Thomas, 1955; Mullins, 1959; Sun et al., 2017), peel (Gent and Lai, 1994; Gent and Hamed, 1977; Gent et al., 1969; Tanaka et al., 2000, 2005, 2016), and pure shear (Baumberger et al., 2006a,b; Baumberger and Ronsin, 2009; Seitz et al., 2009). We choose tear to study time-dependent fracture of a hydrogel of complex rheology for several reasons. First, the tear speed is set by the loading machine. Because the hydrogel is attached with two inextensible backing layers, in steady state, the tear speed v is half of the speed at which the layers are pulled by the loading machine. Consequently, we do not need to measure the tear speed by videotaping the tear front.

Second, the energy release rate of tear is easily measured. The inextensible backing layers suppress deformation in the hydrogel far away from the crack front, so that the energy release rate is

$$G = 2F/h. \tag{1}$$

where F is the tear force, and h is the thickness of the hydrogel. Incidentally, this expression is also valid for peel, where h is replaced by the width of the hydrogel.

Third, the tear path is well guided by the inextensible backing layers for hydrogel of any thickness. Consequently, we can vary the thickness of the hydrogel over a large range to study the effect of thickness. By contrast, precutting a crack in a sample for peel requires the crack front to stay well in the mid-plane of the hydrogel, which is challenging in practice when the thickness of the hydrogel becomes sub-millimeter scale. Also, peel path often runs along, or near, the interface between the hydrogel and a backing layer.

Fourth, the inextensible backing layers localize active deformation of the hydrogel in a region around the tear front. We make the length and width of the hydrogel much larger than the thickness of the hydrogel, so that the thickness of the hydrogel, h, is the only relevant length characteristic of the sample. This region of active deformation, approximately of volume h^3, travels at the tear speed. The hydrogel ahead and behind this active region does not deform. Consequently, at a tear speed v, the time of active deformation of each material particle is estimated by

$$t \approx h/v. \tag{2}$$

This time of active deformation is independent of the rheology of the hydrogel, and is the same for all material particles going through deformation.

Previously reported tear tests on elastomers (ASTM D624-00, 2012; Gent and Lai, 1994; Greensmith and Thomas, 1955; Mullins, 1959; Rivlin and Thomas, 1953) and hydrogels (Sun et al., 2013, 2017) did not use backing layers. Here we use the backing layers to localize the active deformation in a volume scaled by h^3, so that the thickness is the only length scale characterizing the size of the specimen. By changing the thickness, we readily differentiate small-scale and large-scale inelasticity. We study the effect of the thickness relative to the size of the inelastic zone. Besides, the backing layers also enable the tear of very soft materials. The backing layer may modify the stress field near the tear front; we have not studied the difference between tears with and without backing layers.

We prescribe the tear speed v by a loading machine, record the tear force F by a force sensor, and plot the experimental data as a v–G curve (Fig. 5a). The energy release rate approaches a threshold G_0, below which the tear speed vanishes. The existence of the threshold is guaranteed by the primary network: a finite force is needed to break the covalent network no matter how much time the force pulls the primary network.

We hypothesize that the threshold of a tough hydrogel depends on whether the toughener is liquid-like or solid-like. For a tough hydrogel with a liquid-like toughener, the threshold only depends on the primary network, since the liquid-like toughener will be stress-relaxed after some time and will not contribute to the bridging of the crack extending at

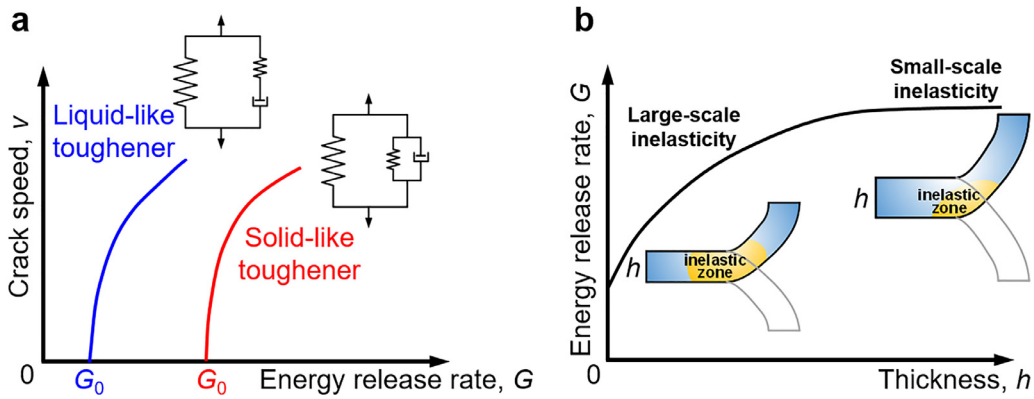

Fig. 5. **(a)** Schematic v–G curves of hydrogels with the same primary network, but solid-like and liquid-like tougheners. **(b)** At a constant tear speed, the energy release rate increases with thickness, and reaches a plateau when the thickness is sufficiently large.

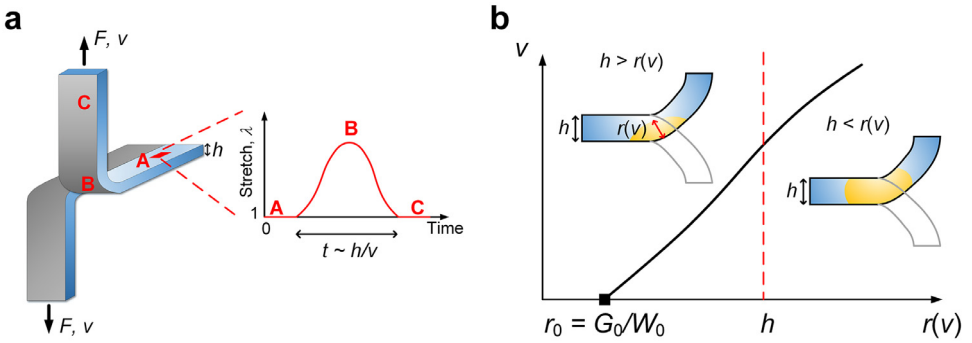

Fig. 6. Mechanics of tear. **(a)** The complete loading-unloading process of a material particle. The time of the loading-unloading process is estimated by $t \sim h/v$. **(b)** A schematic plot indicating that the length $r(v)$ increases with the tear speed v. When $h > r(v)$, energy dissipation takes place within a region of size $r(v)$. When $h < r(v)$, energy dissipation takes place in the entire region of active deformation, of the size scaled by the thickness of hydrogel, h.

a vanishingly low speed. For a tough hydrogel with a solid-like toughener, however, the threshold depends on both the primary network and the toughener, since the solid-like toughener will bear load no matter how slow the crack extends. As a result, with the same primary network, a hydrogel with a solid-like toughener has a higher threshold than a hydrogel with a liquid-like toughener.

Because the thickness of the sample can be readily adjusted over a large range in peel and tear, the two experimental setups can be used to probe the scale of inelasticity. At a constant tear speed, the energy release rate increases with the thickness, and reaches a plateau when the thickness is sufficiently large (Fig. 5b). For a thick sample, the inelastic zone is small compared to the thickness h, small-scale inelasticity prevails, and the energy release rate G does not depend on the thickness h. For a thin sample, the inelastic zone is large compared to the thickness h, large-scale inelasticity prevails, and the energy release rate G increases with the thickness h. In peeling materials like elastomers, plastics and metals, the dependence of peel force on thickness has long been observed experimentally (Gent and Hamed, 1977) and analyzed theoretically (Kim and Aravas, 1988; Wei and Hutchinson, 1998). Similar behavior is expected for tear when the backing layers restrict the zone of active deformation.

As the machine tears the hydrogel, a material particle in the hydrogel undergoes a loading-unloading process (Fig. 6a). Initially, the material particle is far ahead the tear front, and is undeformed (Point A). The material particle deforms as it approaches the tear front, within a distance about h (Point B). Finally, the material particle moves far behind the tear front, and does not deform further (Point C). The time of this entire loading-unloading process is estimated by $t \approx h/v$. For complete relaxation of the toughener, it is required that the time of active deformation, $t \approx h/v$, exceeds the relaxation time of the toughener, τ. In the current study, the largest thickness used is $h = 3.0$ mm, and the lowest tear speed applied is $v = 0.5$ μm/s, so that the longest time of active deformation is estimated by $t \sim 6000$ s ~ 1.7 h, two orders of magnitude smaller than the relaxation time of Ca-alginate, $\tau \sim 12$ days. Therefore, all the current tear tests do not fully relax the Ca-alginate toughener. To obtain the threshold G_0, we conduct linear regression on the three experimental data points of lowest tear speed in each individual v–G curve. Such a way of extrapolation is similar to the extrapolation of thresholds from v–G curves of rubbers, where the lowest measurable crack speed is still far above the speed required for complete viscoelastic relaxation in most cases (Gent and Lai, 1994; Greensmith and Thomas, 1955; Mullins, 1959).

At the threshold G_0, where the tear speed is vanishingly low, the material can be considered as rate-independent. Let W_0 be the work of rupture of the material tested in vanishingly low stretching rate. That is, W_0 is the area under the stress-stretch curve of a sample containing no crack, measured at vanishingly low stretching rate, up to rupture. A material length emerges:

$$r_0 = G_0/W_0. \tag{3}$$

This length was defined for rate-independent materials (Chen et al., 2017). Here we adopt this definition for a material tested at vanishingly low rate. For an ideal elastomer network, this length is estimated to be on the order of the end-to-end distance of a polymer chain in the undeformed elastomer network, $r_0 \approx a\sqrt{n}$, where a is the length of each monomer unit in the polymer chain, and n is the number of monomer units in the polymer chain (Chen et al., 2017). Using representative numbers for a polyacrylamide hydrogel, $a \approx 0.5$ nm, $n \approx 1000$ (Bai et al., 2018), we estimate $r_0 \approx 16$ nm. Real hydrogels, however, have imperfect networks, often leading to much larger length r_0.

When the thickness of the hydrogel is much larger than the material length, $h >> r_0$, following Chen et al. (2017), we expect that the threshold is independent of the thickness of the hydrogel. In our experiments, the thinnest hydrogel is $h = 0.4$ mm. Indeed, our experimental data will confirm that the threshold is independent of the thickness for low concentrations of calcium, but is dependent of the thickness for high concentrations of calcium.

At a finite tear speed v, the measured energy release rate is a function of the prescribed tear speed, $G(v)$. Because time-dependent dissipation from the toughener contributes to the energy release rate, $G(v) > G_0$. For a thick hydrogel, the inelastic zone around the tear front is small compared to the thickness of the hydrogel. Under this condition of small-scale

inelasticity, the size of the inelastic zone is a function of the tear speed, which we denote by $r(v)$. We expect that the v–G curve is independent of the thickness of the hydrogel when the thickness is above the size of the inelastic zone, $h > r(v)$. By definition, $r(0) = r_0$. Furthermore, the length $r(v)$ increases with the tear speed v, and it will exceed the thickness of the hydrogel h when v is large enough or h is small enough. When $h < r(v)$, energy dissipation takes place in the entire region of active deformation, of the size scaled by the thickness of hydrogel, h (Fig. 6b). In tear without backing layers, the active deformation in the sample is not localized in a volume scaled with h^3. In this case, the conditions for small-scale and large-scale inelasticity cannot be determined by simply comparing $r(v)$ and h.

5. The effect of thickness on tear

We prepare hydrogel samples of 0.4, 0.7, 1.0, 1.5 and 3.0 mm thickness. The composition of hydrogel is fixed to the 1-Ca condition ($CaSO_4{\cdot}2H_2O$ of 0.022 times the weight of AAm). During tear, the force F is recorded as a function of the displacement prescribed by the loading machine (Fig. 7). The curve has a transient state at the beginning that is poorly repeatable, followed by a steady state corresponding to a plateau of the curve. We conduct tear over a large range of tear speed from 0.5 μm/s to 10 mm/s. In all cases of different thickness, the force at the steady state increases with the tear speed, consistent with the large rate-dependent hysteresis of the Ca-alginate toughener.

The tear speed v is prescribed by the loading machine at the arms of the sample. The tear front has its own local dynamics, and may or may not advance in a steady state. In our experiment, the measured force-displacement curves jump up and down when the prescribed tear speed v is large, but remain relatively smooth at the plateau when v is small. When the prescribed tear speed is large, the hydrogel undergoes periodic large stretch and sudden rupture at the tear front, accompanied by slight debonding of the backing layers near the tear front, slight twist of the sample arms, and slight vibration of the sample (Fig. 8a, Movie 1). When the prescribed tear speed is small, the hydrogel remains highly stretched at the tear front, but no large sudden rupture occurs (Fig. 8b). In all experiments, the crack path is well guided by the backing layers (Fig. 8c and d). The unsteady stop-jump behavior in the tear experiment is reminiscent of the stick-slip behavior in a sliding experiment. The stick-slip crack growth has been studied in tear and peel of elastomers (ASTM D624-00, 2012; Gent and Pulford, 1984; Greensmith and Thomas, 1955; Maugis, 1985; Mullins, 1959; Veith, 1965). The stick-slip crack growth has

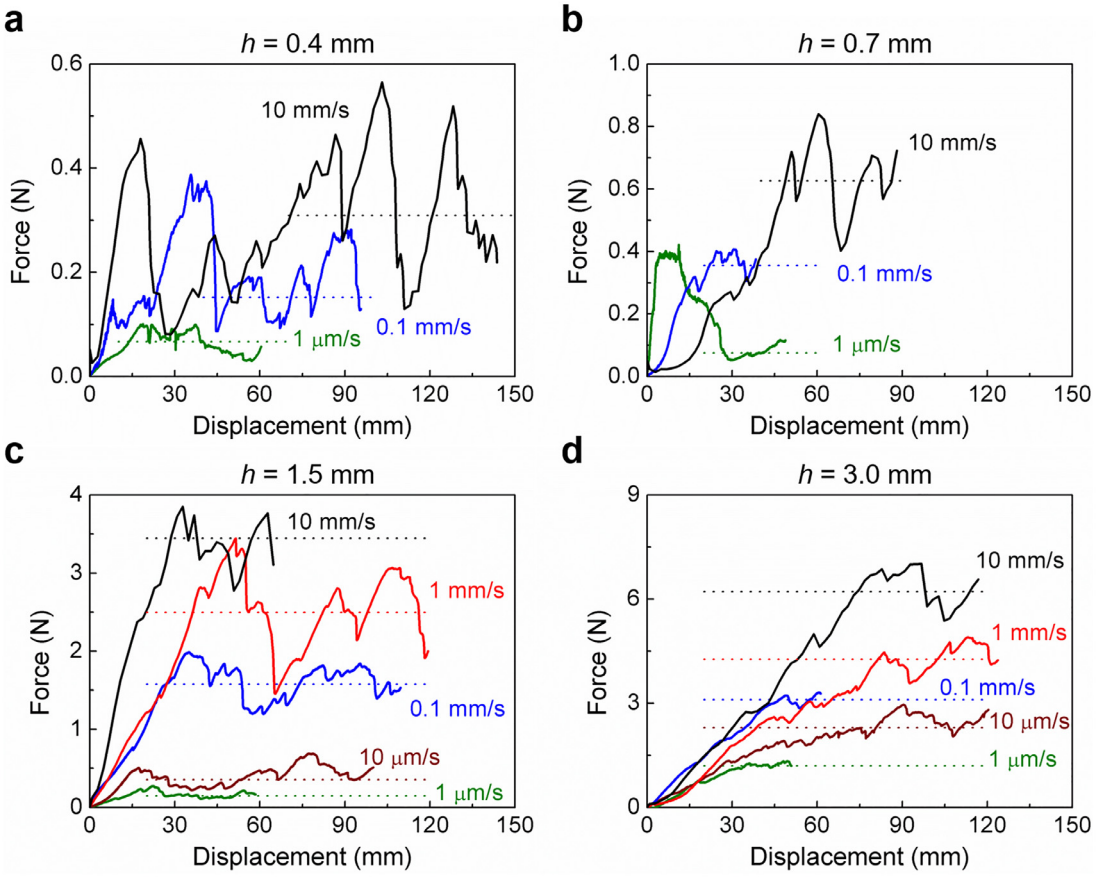

Fig. 7. Representative force-displacement curves from tearing the hydrogels of varied thickness of **(a)** 0.4 mm, **(b)** 0.7 mm, **(c)** 1.5 mm and **(d)** 3.0 mm. The composition of hydrogel is fixed to the 1-Ca condition ($CaSO_4{\cdot}2H_2O$ of 0.022 times the weight of AAm).

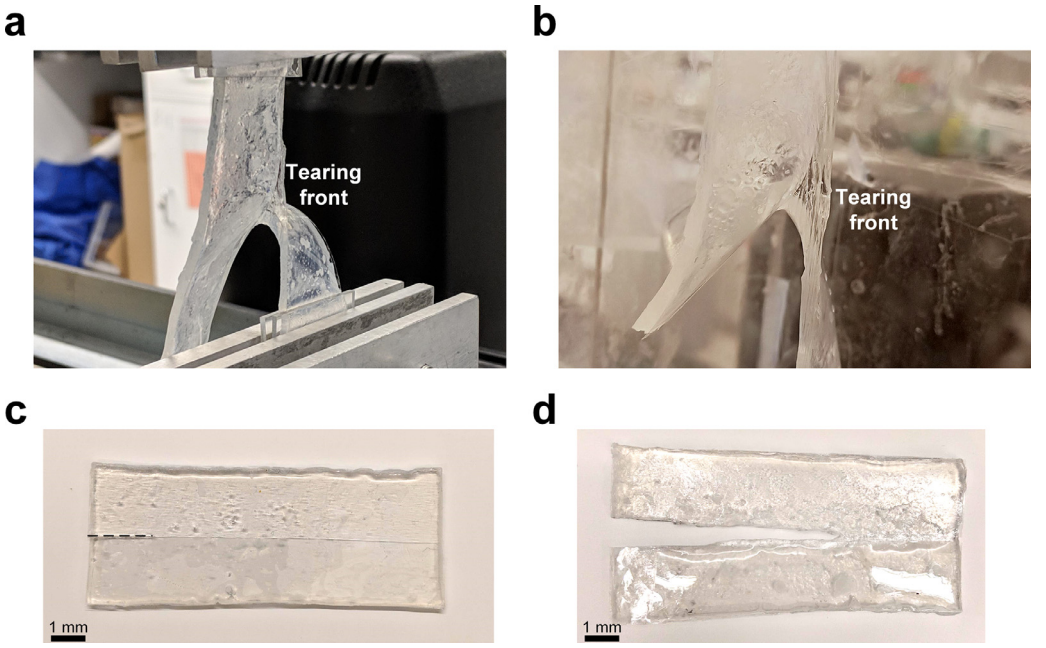

Fig. 8. Photos of tear. **(a)** $h = 3.0$ mm, $v = 2$ mm/s. The hydrogel undergoes periodic large stretch and sudden rupture at the tear front. **(b)** $h = 3.0$ mm, $v = 0.5$ μm/s. The hydrogel remains highly stretched at the tear front and advances in a steady state. No large sudden rupture is observed. **(c)** A sample of hydrogel before tear, a precut crack is made from the left. **(d)** A sample of hydrogel after tear. The crack is well guided by the backing layers.

also been studied in peel of hydrogels (Tanaka et al., 2000, 2016). Here we do not study the stick-slip dynamics, and simply use the average tear force to calculate the energy release rate G.

We record the v–G curves with v ranging from 0.5 μm/s to 10 mm/s, for thickness $h = 0.4$, 0.7, 1.0, 1.5 and 3.0 mm (Fig. 9a). At a high tear speed, the energy release rate greatly increases with h from 0.4, 0.7, 1.0 to 1.5 mm, but keeps almost identical between 1.5 and 3.0 mm. For example, when $v = 10$ mm/s, the energy release rate is about 1500 J/m^2 for $h = 0.4$ mm, 2000 J/m^2 for $h = 0.7$ mm, and 4000 J/m^2 for $h = 1.5$ mm and 3.0 mm. At a low tear speed, however, all the four v–G curves approach almost the same threshold of around 200 J/m^2. For the 1-Ca hydrogel, the energy release rate G depends on the tear speed and sample thickness, but the threshold G_0 depends negligibly on the thickness.

The observed lower energy release rate with the decreasing sample thickness can be of great importance to thin films or coatings of tough hydrogels. Thin films of hydrogels have found broad applications, including soft robots (Acome et al., 2018; Kellaris et al., 2018), artificial skins (Sun et al., 2014; Yuk et al., 2016), medical devices (Parada et al., 2017), living responsive devices (Liu et al., 2018), and chemical sensors (Qin et al., 2018; Sun et al., 2018). Hydrogels become less tough when thickness is small. The v–G curves show that the measured energy release rate of PAAm-Ca-alginate decreases from

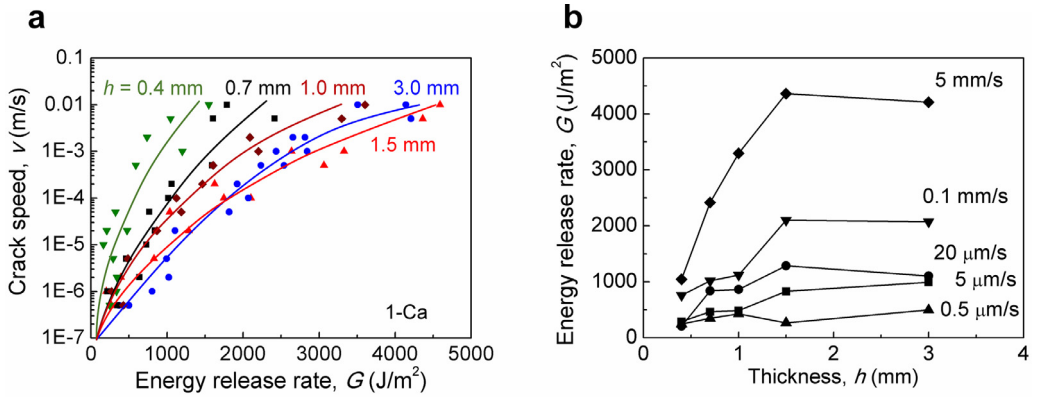

Fig. 9. **(a)** The v–G curves of PAAm-Ca-alginate hydrogels with composition fixed to the 1-Ca condition under five thicknesses. The solid lines are guiding lines for the experimental data. **(b)** The energy release rate G depends negligibly on the thickness h at a tear speed of 0.5 μm/s. At higher tear speeds, G increases with h from 0.4 mm, 0.7 mm, 1.0 mm to 1.5 mm, but reaches a plateau from 1.5 mm to 3.0 mm.

$\sim$2500 J/m^2 to $\sim$700 J/m^2 as the thickness is reduced from 1.5 mm to 400 μm, even when the tear speed is relatively high. The energy release rate approaches the threshold as the tear speed and hydrogel thickness reduce.

We now use the experimental data to estimate the size of inelastic zone, $r(v)$, under the condition of small-scale inelasticity. We plot the energy release rate G as a function of h at different tear speed v (Fig. 9b). When $v = 0.5$ μm/s, G is nearly identical over the full range of h under study. This indicates that $r(0.5\ \mu m/s)$ is smaller than 0.4 mm. When $v > 0.5$ μm/s, G increases with h from 0.4 to 1.0 mm, but reaches a plateau between $h = 1.5$ mm and $h = 3.0$ mm, indicating that $r(v > 0.5\ \mu m/s)$ stays in the range between 1.0 mm and 1.5 mm. As a result, the upper/lower bounds of $r(v)$ are estimated to be

$$\begin{cases} r(v) < 0.4\,\text{mm} & v = 0.5\,\mu\text{m/s} \\ 1.0\,\text{mm} < r(v) < 1.5\,\text{mm} & v = 0.5\,\mu\text{m/s} \end{cases}. \tag{4}$$

A similar dependence of G upon the thickness has been observed in peel of adhesive joints (Gent and Hamed, 1977).

6. The effect of toughener on tear

To study the effect of the Ca-alginate toughener, we fixed the sample thickness to be $h = 1.5$ mm, and synthesized PAAm-alginate hydrogels with the $CaSO_4{\cdot}2H_2O$ amount of 0, 0.022, and 0.044 times the weight of AAm, denoted as the 0-Ca, 1-Ca and 2-Ca hydrogels. We recorded the force-displacement curves (Fig. 10) and the v–G curves (Fig. 11a). For the 0-Ca hydrogel, the alginate chains are uncrosslinked, only interpenetrating the PAAm network. The measured G is low at all tear speeds, and shows little dependence on v compared to the cases of 1-Ca and 2-Ca hydrogels. For the 1-Ca and 2-Ca hydrogels, the energy release rate increases with more calcium added. To illustrate, at $v = 0.01$ m/s, the measured energy release rate is about 250 J/m^2 for the 0-Ca hydrogel, 4500 J/m^2 for the 1-Ca hydrogel, and 10,000 J/m^2 for the 2-Ca hydrogel.

We relate the threshold to the solid-like rheology of the Ca-alginate network. When the tear speed is close to zero, the fully relaxed component cannot contribute to the tear force, but the rate-independent component can. For the 0-Ca hydrogel, the uncrosslinked alginate is liquid-like, making negligible contribution to the threshold. Consequently, the measured value $G_0|_{0-Ca} = 59$ J/m^2 is entirely due to the PAAm network. For the 1-Ca and the 2-Ca hydrogels, the thresholds are

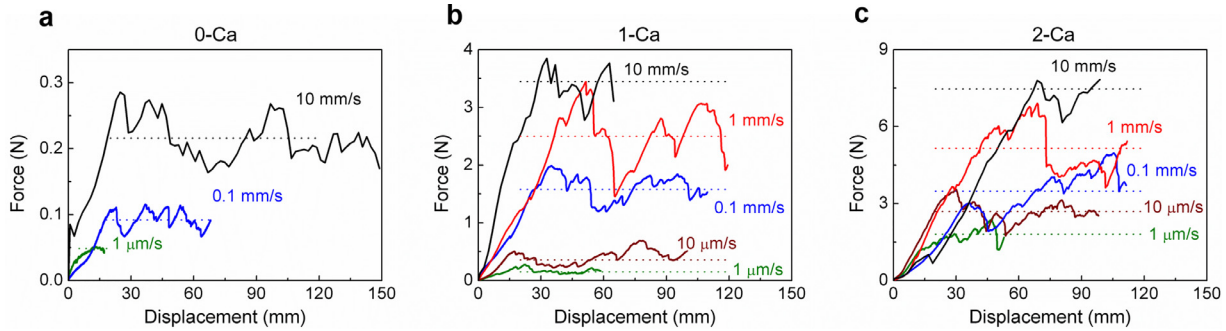

Fig. 10. Representative force-displacement curves of PAAm-alginate hydrogels with different amounts of calcium, the same thickness $h = 1.5$ mm. **(a)** 0-Ca: no calcium. **(b)** 1-Ca: $CaSO_4{\cdot}2H_2O$ of 0.022 times the weight of AAm. **(c)** 2-Ca: $CaSO_4{\cdot}2H_2O$ of 0.044 times the weight of AAm.

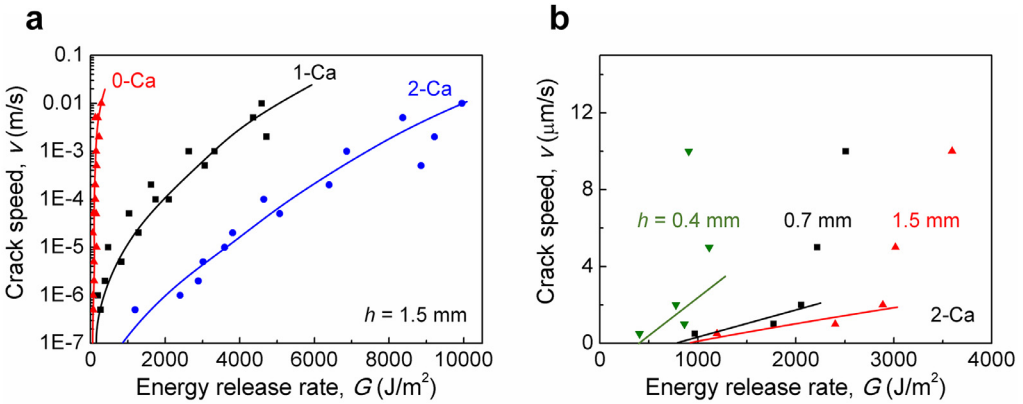

Fig. 11. **(a)** v–G curves of PAAm-Ca-alginate hydrogels with $h = 1.5$ mm and different amounts of calcium. The threshold G_0 is calculated to be 59, 173 and 952 J/m^2 for the 0-Ca, 1-Ca and 2-Ca hydrogel, respectively. **(b)** v–G curves of PAAm-Ca-alginate hydrogels with fixed composition of 2-Ca and different thicknesses. The threshold G_0 is calculated to be 446, 830 and 952 J/m^2 for $h = 0.4$, 0.7, and 1.5 mm, respectively. In each curve of (a) and (b), the threshold is calculated by linear regression of the three smallest data points.

$G_0|_{1-Ca} = 173\,J/m^2$ and $G_0|_{2-Ca} = 952\,J/m^2$. Because the PAAm networks in the three hydrogels are identical, the increase in the threshold is due to the presence of Ca-alginate. The increase in the threshold, however, does not come from the scission of alginate chains, but from unzipping of calcium bonds over a finite volume surrounding the tear front. Even at the vanishingly low tear speed, the unrelaxed Ca-alginate network can still undergo hysteresis as material particles undergo the loading-unloading process.

For the 2-Ca hydrogels, even at the threshold with vanishingly low tear speed, the solid-like Ca-alginate network amplifies the inelastic zone so large to be comparable to the thickness. Consequently, large-scale inelasticity prevails at the threshold. The threshold G_0 is 446, 830 and 952 J/m^2 for $h = 0.4$, 0.7, and 1.5 mm, respectively (Fig. 11b).

7. Discussion

The condition of large-scale inelasticity complicates the definition of energy release rate in most experimental setups. Rather, the extension of a crack in a material of complex rheology can be analyzed by the cohesive zone model, where the "cohesion" of the material at the crack front is represented by a traction-displacement model, and the dissipation in the bulk is represented by a rheological model (Needleman, 1987; Schapery, 1975; Tvergaard and Hutchinson, 1992). This approach has recently been adopted in the study of hydrogels (Baumberger et al., 2006b; Lefranc and Bouchaud, 2014; Long and Hui, 2015, 2016; Noselli et al., 2016; Qi et al., 2018; Yu et al., 2018; Zhang et al., 2015).

In the literature on elastomers, efforts have long been made to study the "decohesion"—the scission of the polymer network at the crack front—by conducting experiments that minimize the dissipation from the bulk (Lake and Thomas, 1967). Such experiments include fatigue fracture and slow crack. Fatigue fracture is conducted under cyclic loads (Lake and Thomas, 1967; Thomas, 1958), where the crack extension per cycle dc/dN in a pre-cut sample is measured as a function of the energy release rate G. The threshold for fatigue fracture is the finite G value when dc/dN approaches zero. Slow crack is conducted under monotonic loads (Gent and Lai, 1994; Greensmith and Thomas, 1955; Mullins, 1959), where the crack speed v is a function of the energy release rate G. The threshold for slow crack is the finite G value when the crack speed approaches zero.

Studies on the "decohesion" of hydrogels have also started. Zhang et al. (2015) measured the fracture energy of a polyacrylamide-calcium-alginate hydrogel by first prescribing a large pre-stretch to unzip the ionic crosslinks of the alginate network, and then measuring the fracture energy. Fatigue fracture has been recently tested for hydrogels including polyacrylamide (PAAm) (Tang et al., 2017; Zhang et al., 2018a), polyacrylamide-calcium-alginate (PAAm-Ca-alginate) (Bai et al., 2017; Zhang et al., 2018b), polyacrylamide-poly(2-acrylamido-2-methylpropane sulfonic acid) (PAAm-PAMPS) (Zhang et al., 2018c), and polyacrylamide-poly(vinyl alcohol) (PAAm-PVA) (Bai et al., 2018). The threshold for fatigue fracture depends on the primary network (e.g., the polyacrylamide network), but negligibly on the toughener, either solid-like (Zhang et al., 2018b) or liquid-like (Bai et al., 2018). Slow crack has been conducted for non-covalently crosslinked hydrogels such as gelatin and Ca-alginate (Baumberger et al., 2006b; Baumberger and Ronsin, 2009). The threshold for slow crack of these hydrogels corresponds to the breaking of the noncovalent crosslinks. Slow crack has also been conducted for hydrogels with stronger ionic crosslinks (Sun et al., 2017) or covalent crosslinks (Tanaka et al., 2000, 2005; Yang et al., 2018), but has been focused on the toughening mechanism above the threshold, instead of the threshold itself.

In the literature, it has been unclear whether the fatigue-crack threshold and the slow-crack threshold are identical. There has been no direct comparison of the two thresholds. Our own experimental data indicate that they are not identical. The fatigue-crack threshold of a PAAm-Ca-alginate hydrogel with identical composition of the PAAm network used in this paper has been measured in our previous work (Bai et al., 2017). The measured fatigue-crack threshold of the PAAm-Ca-alginate hydrogel is close to the slow-crack threshold of the 0-Ca hydrogel in the current paper. That is, the Ca-alginate contributes negligibly to the fatigue-crack threshold, but contributes substantially to the slow-crack threshold. The comparison between the thresholds measured under these different conditions calls for future investigation.

8. Conclusion

Tough hydrogels of various compositions exhibit complex rheology, which complicates the link between the mechanics of fracture and the chemistry of hydrogels. In this paper, we study PAAm-Ca-alginate hydrogels by tear, where the tear speed and the energy release rate are readily determined, independent of the rheology of the hydrogels. The energy release rate G decreases as the tear speed v decreases, and reaches a threshold when the tear speed vanishes. The v–G curve depends on both the thickness of the hydrogel and the concentration of calcium. The thickness-dependence reflects the condition of large-scale inelasticity. The threshold depends on the concentration of calcium. The threshold may or may not depend on the thickness, depending on the thickness relative to the size of the inelastic zone. A stress relaxation test shows that the Ca-alginate network exhibits solid-like rheology. We find that Ca-alginate contributes substantially to slow-crack threshold, but negligibly to fatigue-crack threshold. It is hoped that tear of other tough hydrogels will soon be studied and compared with fatigue fracture of these hydrogels.

Acknowledgment

This work was supported by NSF MRSEC (DMR-14-20570).

Supplementary material

Supplementary material associated with this article can be found, in the online version, at doi:10.1016/j.jmps.2019.01.017.

References

Acome, E., Mitchell, S.K., Morrissey, T.G., Emmett, M.B., Benjamin, C., King, M., Radakovitz, M., Keplinger, C., 2018. Hydraulically amplified self-healing electrostatic actuators with muscle-like performance. Science 359, 61–65.

ASTM D624-00, 2012. Standard Test Method for Tear Strength of Conventional Vulcanized Rubber and Thermoplastic Elastomers. ASTM International, West Conshohocken, PA www.astm.org.

Bai, R., Yang, J., Morelle, X.P., Yang, C., Suo, Z., 2018. Fatigue fracture of self-recovery hydrogels. ACS Macro Lett. 312–317.

Bai, R., Yang, J., Suo, Z., 2019. Fatigue of hydrogels. Eur. J. Mech. 74, 337–370.

Bai, R., Yang, Q., Tang, J., Morelle, X.P., Vlassak, J., Suo, Z., 2017. Fatigue fracture of tough hydrogels. Extreme Mech. Lett. 15, 91–96.

Bajpai, S., Sharma, S., 2004. Investigation of swelling/degradation behaviour of alginate beads crosslinked with Ca^{2+} and Ba^{2+} ions. React. Funct. Polym. 59, 129–140.

Baumberger, T., Caroli, C., Martina, D., 2006a. Fracture of a biopolymer gel as a viscoplastic disentanglement process. Eur. Phys. J. E 21, 81–89.

Baumberger, T., Caroli, C., Martina, D., 2006b. Solvent control of crack dynamics in a reversible hydrogel. Nat. Mater. 5, 552–555.

Baumberger, T., Ronsin, O., 2009. From thermally activated to viscosity controlled fracture of biopolymer hydrogels. J. Chem. Phys. 130, 061102.

Baumberger, T., Ronsin, O., 2010. A convective instability mechanism for quasistatic crack branching in a hydrogel. Eur. Phys. J. E 31, 51–58.

Bonn, D., Kellay, H., Prochnow, M., Ben-Djemiaa, K., Meunier, J., 1998. Delayed fracture of an inhomogeneous soft solid. Science 280, 265–267.

Braccini, I., Pérez, S., 2001. Molecular basis of Ca2+-induced gelation in alginates and pectins: the egg-box model revisited. Biomacromolecules 2, 1089–1096.

Caló, E., Khutoryanskiy, V.V., 2015. Biomedical applications of hydrogels: a review of patents and commercial products. Eur. Polym. J. 65, 252–267.

Chen, C., Wang, Z., Suo, Z., 2017. Flaw sensitivity of highly stretchable materials. Extreme Mech. Lett. 10, 50–57.

Choi, M., Humar, M., Kim, S., Yun, S.H., 2015. Step-index optical fiber made of biocompatible hydrogels. Adv. Mater. 27, 4081–4086.

Creton, C., 2017. 50th anniversary perspective: networks and gels: soft but dynamic and tough. Macromolecules 50, 8297–8316.

Du, G., Gao, G., Hou, R., Cheng, Y., Chen, T., Fu, J., Fei, B., 2014. Tough and fatigue resistant biomimetic hydrogels of interlaced self-assembled conjugated polymer belts with a polyelectrolyte network. Chem. Mater. 26, 3522–3529.

Evans, A.G., 1990. Perspective on the development of high-toughness ceramics. J. Am. Ceram. Soc. 73, 187–206.

Gent, A., Lai, S.M., 1994. Interfacial bonding, energy dissipation, and adhesion. J. Polym. Sci., Part B 32, 1543–1555.

Gent, A.N., Hamed, G.R., 1977. Peel mechanics of adhesive joints. Polym. Eng. Sci. 17, 462–466.

Gent, A.N., Petrich, R.P., Tabor, D., 1969. Adhesion of viscoelastic materials to rigid substrates. Proc. R. Soc. Lond. 310, 433–448.

Gent, A.N., Pulford, C.T.R., 1984. Micromechanics of fracture in elastomers. J. Mater. Sci. 19, 3612–3619.

Gong, J.P., 2010. Why are double network hydrogels so tough? Soft Matter 6, 2583–2590.

Gong, J.P., Katsuyama, Y., Kurokawa, T., Osada, Y., 2003. Double-network hydrogels with extremely high mechanical strength. Adv. Mater. 15, 1155–1158.

Greensmith, H.W., Thomas, A.G., 1955. Rupture of rubber. III. Determination of tear properties. J. Polym. Sci. 18, 189–200.

Guo, J., Liu, X., Jiang, N., Yetisen, A.K., Yuk, H., Yang, C., Khademhosseini, A., Zhao, X., Yun, S.H., 2016. Highly stretchable, strain sensing hydrogel optical fibers. Adv. Mater. 28, 10244–10249.

Haque, M.A., Kurokawa, T., Gong, J.P., 2012a. Anisotropic hydrogel based on bilayers: color, strength, toughness, and fatigue resistance. Soft Matter 8, 8008–8016.

Haque, M.A., Kurokawa, T., Gong, J.P., 2012b. Super tough double network hydrogels and their application as biomaterials. Polymer 53, 1805–1822.

Hashimoto, W., Mishima, Y., Miyake, O., Nankai, H., Momma, K., Murata, K., Matsumura, S., Steinbüchel, A., 2005. Biodegradation of Alginate, Xanthan, and Gellan. A. Steinbüchel.

Hu, X., Vatankhah-Varnoosfaderani, M., Zhou, J., Li, Q., Sheiko, S.S., 2015. Weak hydrogen bonding enables hard, strong, tough, and elastic hydrogels. Adv. Mater. 27, 6899–6905.

Huang, Y., King, D.R., Sun, T.L., Nonoyama, T., Kurokawa, T., Nakajima, T., Gong, J.P., 2017. Energy-dissipative matrices enable synergistic toughening in fiber reinforced soft composites. Adv. Funct. Mater. 27.

Illeperuma, W.R., Rothemund, P., Suo, Z., Vlassak, J.J., 2016. Fire-resistant hydrogel-fabric laminates: a simple concept that may save lives. ACS Appl. Mater. Inter. 8, 2071–2077.

Illeperuma, W.R., Sun, J.-Y., Suo, Z., Vlassak, J.J., 2014. Fiber-reinforced tough hydrogels. Extreme Mech. Lett. 1, 90–96.

Jeon, I., Cui, J., Illeperuma, W.R., Aizenberg, J., Vlassak, J.J., 2016. Extremely stretchable and fast self-healing hydrogels. Adv. Mater. 28, 4678–4683.

Karobi, S.N., Sun, T.L., Kurokawa, T., Luo, F., Nakajima, T., Nonoyama, T., Gong, J.P., 2016. Creep behavior and delayed fracture of tough polyampholyte hydrogels by tensile test. Macromolecules 49, 5630–5636.

Kellaris, N., Venkata, V.G., Smith, G.M., Mitchell, S.K., Keplinger, C., 2018. Peano-HASEL actuators: muscle-mimetic, electrohydraulic transducers that linearly contract on activation. Sci. Robot. 3, eaar3276.

Keplinger, C., Sun, J.Y., Foo, C.C., Rothemund, P., Whitesides, G.M., Suo, Z., 2013. Stretchable, transparent, ionic conductors. Science 341, 984–987.

Kim, C.C., Lee, H.H., Oh, K.H., Sun, J.Y., 2016. Highly stretchable, transparent ionic touch panel. Science 353, 682–687.

Kim, K.S., Aravas, N., 1988. Elastoplastic analysis of the peel test. Int. J. Solids Struct. 24, 417–435.

Lake, G., Thomas, A., 1967. The strength of highly elastic materials. Proc. R. Soc. London, Ser. A 300, 108–119.

Larson, C., Peele, B., Li, S., Robinson, S., Totaro, M., Beccai, L., Mazzolai, B., Shepherd, R., 2016. Highly stretchable electroluminescent skin for optical signaling and tactile sensing. Science 351, 1071–1074.

Le Floch, P., Yao, X., Liu, Q., Wang, Z., Nian, G., Sun, Y., Jia, L., Suo, Z., 2017. Wearable and washable conductors for active textiles. ACS Appl. Mater. Inter. 9, 25542–25552.

Lefranc, M., Bouchaud, E., 2014. Mode I fracture of a biopolymer gel: rate-dependent dissipation and large deformations disentangled. Extreme Mech. Lett. 1, 97–103.

Lei, Z., Wang, Q., Sun, S., Zhu, W., Wu, P., 2017. A bioinspired mineral hydrogel as a self-healable, mechanically adaptable ionic skin for highly sensitive pressure sensing. Adv. Mater. 29.

Li, J., Celiz, A.D., Yang, J., Yang, Q., Wamala, I., Whyte, W., Seo, B.R., Vasilyev, N.V., Vlassak, J.J., Suo, Z., Mooney, D.J., 2017a. Tough adhesives for diverse wet surfaces. Science 357, 378–381.

Li, J., Illeperuma, W.R.K., Suo, Z., Vlassak, J.J., 2014. Hybrid hydrogels with extremely high stiffness and toughness. ACS Macro Lett. 3, 520–523.

Li, J., Mooney, D.J., 2016. Designing hydrogels for controlled drug delivery. Nat. Rev. Mater. 1, 16071.

Li, T., Li, G., Liang, Y., Cheng, T., Dai, J., Yang, X., Liu, B., Zeng, Z., Huang, Z., Luo, Y., 2017b. Fast-moving soft electronic fish. Sci. Adv. 3, e1602045.

Lin, S., Cao, C., Wang, Q., Gonzalez, M., Dolbow, J.E., Zhao, X., 2014. Design of stiff, tough and stretchy hydrogel composites via nanoscale hybrid crosslinking and macroscale fiber reinforcement. Soft Matter 10, 7519–7527.

Liu, J., Pang, Y., Zhang, S., Cleveland, C., Yin, X., Booth, L., Lin, J., Lucy Lee, Y.A., Mazdiyasni, H., Saxton, S., Kirtane, A.R., Erlach, T.V., Rogner, J., Langer, R., Traverso, G., 2017. Triggerable tough hydrogels for gastric resident dosage forms. Nat. Commun. 8, 124.

Liu, X., Yuk, H., Lin, S., Parada, G.A., Tang, T.C., Tham, E., de la Fuente-Nunez, C., Lu, T.K., Zhao, X., 2018. 3D Printing of living responsive materials and devices. Adv. Mater. 30.

Long, R., Hui, C.-Y., 2015. Crack tip fields in soft elastic solids subjected to large quasi-static deformation—a review. Extreme Mech. Lett. 4, 131–155.
Long, R., Hui, C.Y., 2016. Fracture toughness of hydrogels: measurement and interpretation. Soft Matter 12, 8069–8086.
Mao, Y., Anand, L., 2018. A theory for fracture of polymeric gels. J. Mech. Phys. Solids 115, 30–53.
Mao, Y., Lin, S., Zhao, X., Anand, L., 2017. A large deformation viscoelastic model for double-network hydrogels. J. Mech. Phys. Solids 100, 103–130.
Masuda, F., 1994. Trends in the Development of Superabsorbent Polymers for Diapers, Superabsorbent Polymers. American Chemical Society, pp. 88–98.
Maugis, D., 1985. Subcritical crack growth, surface energy, fracture toughness, stick-slip and embrittlement. J. Mater. Sci. 20, 3041–3073.
Mitchell, J., Blanshard, J., 1976. Rheological properties of alginate gels. J. Texture Stud. 7, 219–234.
Mullins, L., 1959. Rupture of rubber. IX. Role of hysteresis in the tearing of rubber. Trans. Inst. Rubber Ind. 35, 213–222.
Needleman, A., 1987. A continuum model for void nucleation by inclusion debonding. J. Appl. Mech. 54, 525–531.
Noselli, G., Lucantonio, A., McMeeking, R.M., DeSimone, A., 2016. Poroelastic toughening in polymer gels: a theoretical and numerical study. J. Mech. Phys. Solids 94, 33–46.
Parada, G.A., Yuk, H., Liu, X., Hsieh, A.J., Zhao, X., 2017. Impermeable robust hydrogels via hybrid lamination. Adv. Healthc. Mater. 6.
Parida, K., Kumar, V., Jiangxin, W., Bhavanasi, V., Bendi, R., Lee, P.S., 2017. Highly transparent, stretchable, and self-healing ionic-skin triboelectric nanogenerators for energy harvesting and touch applications. Adv. Mater. 29.
Pu, X., Liu, M., Chen, X., Sun, J., Du, C., Zhang, Y., Zhai, J., Hu, W., Wang, Z.L., 2017. Ultrastretchable, transparent triboelectric nanogenerator as electronic skin for biomechanical energy harvesting and tactile sensing. Sci. Adv. 3, e1700015.
Qi, Y., Caillard, J., Long, R., 2018. Fracture toughness of soft materials with rate-independent hysteresis. J. Mech. Phys. Solids 118, 341–364.
Qin, M., Sun, M., Bai, R., Mao, Y., Qian, X., Sikka, D., Zhao, Y., Qi, H.J., Suo, Z., He, X., 2018. Bioinspired hydrogel interferometer for adaptive coloration and chemical sensing. Adv. Mater., 1800468.
Rivlin, R., Thomas, A., 1953. Rupture of rubber. I. Characteristic energy for tearing. J. Polym. Sci. 10, 291–318.
Sarwar, M.S., Dobashi, Y., Preston, C., Wyss, J.K., Mirabbasi, S., Madden, J.D.W., 2017. Bend, stretch, and touch: locating a finger on an actively deformed transparent sensor array. Sci. Adv. 3, e1602200.
Schapery, R.A., 1975. A theory of crack initiation and growth in viscoelastic media. Int. J. Fracture 11, 141–159.
Schroeder, T.B., Guha, A., Lamoureux, A., VanRenterghem, G., Sept, D., Shtein, M., Yang, J., Mayer, M., 2017. An electric-eel-inspired soft power source from stacked hydrogels. Nature 552, 214.
Seitz, M.E., Martina, D., Baumberger, T., Krishnan, V.R., Hui, C.-Y., Shull, K.R., 2009. Fracture and large strain behavior of self-assembled triblock copolymer gels. Soft Matter 5, 447–456.
Sikorski, P., Mo, F., Skjåk-Bræk, G., Stokke, B.T., 2007. Evidence for egg-box-compatible interactions in calcium− alginate gels from fiber X-ray diffraction. Biomacromolecules 8, 2098–2103.
Sun, J.Y., Keplinger, C., Whitesides, G.M., Suo, Z., 2014. Ionic skin. Adv. Mater. 26, 7608–7614.
Sun, J.Y., Zhao, X., Illeperuma, W.R., Chaudhuri, O., Oh, K.H., Mooney, D.J., Vlassak, J.J., Suo, Z., 2012. Highly stretchable and tough hydrogels. Nature 489, 133–136.
Sun, M., Bai, R., Yang, X., Song, J., Qin, M., Suo, Z., He, X., 2018. Hydrogel interferometry for ultrasensitive and highly selective chemical detection. Adv. Mater. 0, 1804916.
Sun, T.L., Kurokawa, T., Kuroda, S., Ihsan, A.B., Akasaki, T., Sato, K., Haque, M.A., Nakajima, T., Gong, J.P., 2013. Physical hydrogels composed of polyampholytes demonstrate high toughness and viscoelasticity. Nat. Mater. 12, 932–937.
Sun, T.L., Luo, F., Hong, W., Cui, K., Huang, Y., Zhang, H.J., King, D.R., Kurokawa, T., Nakajima, T., Gong, J.P., 2017. Bulk energy dissipation mechanism for the fracture of tough and self-healing hydrogels. Macromolecules 50, 2923–2931.
Tanaka, Y., Fukao, K., Miyamoto, Y., 2000. Fracture energy of gels. Eur. Phys. J. E 3, 395–401.
Tanaka, Y., Kuwabara, R., Na, Y.-H., Kurokawa, T., Gong, J.P., Osada, Y., 2005. Determination of fracture energy of high strength double network hydrogels. J. Phys. Chem. B 109, 11559–11562.
Tanaka, Y., Shimazaki, R., Yano, S., Yoshida, G., Yamaguchi, T., 2016. Solvent effects on the fracture of chemically crosslinked gels. Soft Matter 12, 8135–8142.
Tang, J., Li, J., Vlassak, J.J., Suo, Z., 2017. Fatigue fracture of hydrogels. Extreme Mech. Lett. 10, 24–31.
Thomas, A., 1958. Rupture of rubber. V. Cut growth in natural rubber vulcanizates. J. Polym. Sci. 31, 467–480.
Tvergaard, V., Hutchinson, J.W., 1992. The relation between crack growth resistance and fracture process parameters in elastic-plastic solids. J. Mech. Phys. Solids 40, 1377–1397.
Veith, A.G., 1965. A new tear test for rubber. Rubber Chem. Technol. 38, 700–718.
Wang, X., Hong, W., 2012. Delayed fracture in gels. Soft Matter 8, 8171–8178.
Wei, Y., Hutchinson, J.W., 1998. Interface strength, work of adhesion and plasticity in the peel test. In: Knauss, W.G., Schapery, R.A. (Eds.), Recent Advances in Fracture Mechanics: Honoring Mel and Max Williams. Springer, Netherlands, Dordrecht, pp. 315–333.
Wichterle, O., Lim, D., 1960. Hydrophilic gels for biological use. Nature 185, 117.
Wichterle, O., Lim, D., 1961. Process for producing shaped articles from three-dimensional hydrophilic high polymers. US Patent 2,976,576.
Xu, W., Huang, L.B., Wong, M.C., Chen, L., Bai, G., Hao, J., 2017. Environmentally friendly hydrogel-based triboelectric nanogenerators for versatile energy harvesting and self-powered sensors. Adv. Energy Mater. 7.
Yang, C., Suo, Z., 2018. Hydrogel ionotronics. Nat. Rev. Mater. 1.
Yang, C.H., Chen, B., Lu, J.J., Yang, J.H., Zhou, J., Chen, Y.M., Suo, Z., 2015. Ionic cable. Extreme Mech. Lett. 3, 59–65.
Yang, C.H., Chen, B., Zhou, J., Chen, Y.M., Suo, Z., 2016a. Electroluminescence of giant stretchability. Adv. Mater. 28, 4480–4484.
Yang, C.H., Wang, M.X., Haider, H., Yang, J.H., Sun, J.-Y., Chen, Y.M., Zhou, J., Suo, Z., 2013. Strengthening alginate/polyacrylamide hydrogels using various multivalent cations. ACS Appl. Mater. Inter. 5, 10418–10422.
Yang, C.H., Zhou, S., Shian, S., Clarke, D.R., Suo, Z., 2017. Organic liquid-crystal devices based on ionic conductors. Mater. Horiz. 4, 1102–1109.
Yang, J., Bai, R., Suo, Z., 2018. Topological adhesion of wet materials. Adv. Mater. 30, 1800671.
Yang, Y., Wang, X., Yang, F., Shen, H., Wu, D., 2016b. A universal soaking strategy to convert composite hydrogels into extremely tough and rapidly recoverable double-network hydrogels. Adv. Mater. 28, 7178–7184.
Yu, Y., Landis, C.M., Huang, R., 2018. Steady-state crack growth in polymer gels: a linear poroelastic analysis. J. Mech. Phys. Solids 118, 15–39.
Yuk, H., Lin, S., Ma, C., Takaffoli, M., Fang, N.X., Zhao, X., 2017. Hydraulic hydrogel actuators and robots optically and sonically camouflaged in water. Nat. Commun. 8, 14230.
Yuk, H., Zhang, T., Parada, G.A., Liu, X., Zhao, X., 2016. Skin-inspired hydrogel-elastomer hybrids with robust interfaces and functional microstructures. Nat. Commun. 7, 12028.
Zhang, E., Bai, R., Morelle, X.P., Suo, Z., 2018a. Fatigue fracture of nearly elastic hydrogels. Soft Matter 14, 3563–3571.
Zhang, T., Lin, S., Yuk, H., Zhao, X., 2015. Predicting fracture energies and crack-tip fields of soft tough materials. Extreme Mech. Lett. 4, 1–8.
Zhang, W., Hu, J., Tang, J., Wang, Z., Wang, J., Lu, T., Suo, Z., 2018b. Fracture toughness and fatigue threshold of tough hydrogels. ACS Macro Lett. 17–23.
Zhang, W., Liu, X., Wang, J., Tang, J., Hu, J., Lu, T., Suo, Z., 2018c. Fatigue of double-network hydrogels. Eng. Fract. Mech. 187, 74–93.
Zhang, Y.S., Khademhosseini, A., 2017. Advances in engineering hydrogels. Science 356.
Zhao, X., 2014. Multi-scale multi-mechanism design of tough hydrogels: building dissipation into stretchy networks. Soft Matter 10, 672–687.
Zhao, X., Huebsch, N., Mooney, D.J., Suo, Z., 2010. Stress-relaxation behavior in gels with ionic and covalent crosslinks. J. Appl. Phys. 107, 63509.